SCISPACE
formerly Typeset

Open access • Journal Article • DOI:10.1115/1.3662286

On the Mechanism of Cavitation Damage by Nonhemispherical Cavities Collapsing in Contact With a Solid Boundary — Source link

Charl F. Naudé, Albert T. Ellis

Institutions: California Institute of Technology

Published on: 01 Dec 1961 - Journal of Basic Engineering (American Society of Mechanical Engineers)

Topics: Cavity wall and Cavitation

Related papers:

- Collapse of an initially spherical vapour cavity in the neighbourhood of a solid boundary
- VIII. On the pressure developed in a liquid during the collapse of a spherical cavity
- The Collapse of Cavitation Bubbles and the Pressures thereby Produced against Solid Boundaries
- Experimental investigations of cavitation-bubble collapse in the neighbourhood of a solid boundary
- Mechanisms of impulsive pressure generation and damage pit formation by bubble collapse

Share this paper:

View more about this paper here: https://typeset.io/papers/on-the-mechanism-of-cavitation-damage-by-nonhemispherical-45os4h1oqo

On the Mechanism of Cavitation Damage by Nonhemispherical Cavities Collapsing in Contact With a Solid Boundary[1]

CHARL F. NAUDÉ
Research Engineer.

ALBERT T. ELLIS
Associate Professor of Applied Mechanics.
California Institute of Technology, Pasadena, Calif.

A perfect fluid theory, which neglects the effect of gravity, and which assumes that the pressure inside a cavitation bubble remains constant during the collapse process, is given for the case of a nonhemispherical, but axially symmetric cavity which collapses in contact with a solid boundary. The theory suggests the possibility that such a cavity may deform to the extent that its wall strikes the solid boundary before minimum cavity volume is reached. High-speed motion pictures of cavities generated by spark methods are used to test the theory experimentally. Agreement between theory and experiment is good for the range of experimental cavities considered, and the phenomenon of the cavity wall striking the solid boundary does indeed occur. Studies of damage by cavities of this type on soft aluminum samples reveals that pressures caused by the cavity wall striking the boundary are higher than those resulting from a compression of gases inside the cavity, and are responsible for the damage.

Introduction

Until the present, most of the theoretical efforts to explain damage by cavitation were spent in attempts to understand the collapse process of spherical cavities in an infinite liquid. This problem is complicated because effects of compressibility, surface tension, and viscosity play an important role. Furthermore, the behavior of the gaseous substances inside the cavity, and especially the nonequilibrium behavior of the included vapor under high rates of compression are not known.

It has been realized for some time that the spherical shape of a collapsing cavity is unstable in the sense that a finite initial perturbation of the spherical shape will grow very large as the cavity collapses. This instability is demonstrated elegantly in a publication by Plesset and Mitchell [1].[2]

In view of the asymmetric perturbing influences which act on a cavity collapsing close to, or in contact with, a solid boundary it appears reasonable to expect that cavities which do not remain spherically symmetric during collapse could play an important role in cavitation damage. Eisenberg [2] recognized the possibility in 1950 when he speculated that jets formed during the unsymmetrical collapse of cavitation bubbles could be responsible for the damage. Kornfeld and Suvorov [3] also suggested this mechanism of damage in a 1944 publication.

The object of the present study is to investigate the collapse process of, and the mechanism of damage by, cavities in contact with a solid boundary which collapse nonhemispherically mainly as a result of initial perturbations of the hemispherical shape. It is hoped that such a study may be the first step in understanding the mechanism of damage by cavities which collapse nonhemispherically as a result of other effects.

[1] Condensed from a 1960 California Institute of Technology PhD thesis by C. F. Naudé.

[2] Numbers in brackets designate References at end of paper.

Contributed by the Cavitation Subcommittee of the Hydraulic Division of The American Society of Mechanical Engineers and presented at the ASME-EIC Hydraulic Conference, Montreal, Canada, May 7–10, 1961. Manuscript received at ASME Headquarters, January 30, 1961. Paper No. 61—Hyd-8.

Theory

Consider a cavity which is symmetric about a line normal to a solid plane boundary. A spherical co-ordinate system as shown in Fig. 1 is chosen for the formulation of the problem.

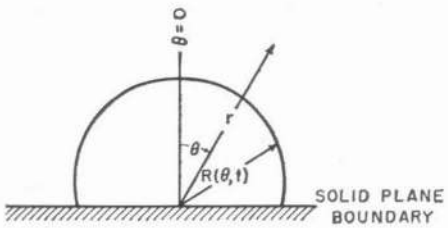

Fig. 1 The spherical co-ordinate system

The following assumptions will be used:

1 The liquid is incompressible.
2 The pressure inside the cavity is constant.
3 The effect of viscosity is negligible.
4 Surface tension and adhesion are negligible.
5 The effect of gravity is negligible.

A brief discussion of the validity of the assumptions follows at the end of the theoretical work.

With the assumptions listed above the problem is reduced to solving the differential equation

$$\nabla^2\Phi(r, \theta, t) = 0 \tag{1}$$

where Φ is a scalar potential function such that $\nabla\Phi = q$, the velocity vector. The following boundary conditions must be satisfied:

$$\Phi \to 0 \quad \text{as} \quad r \to \infty \tag{2}$$

$$\frac{1}{r}\frac{\partial\Phi}{\partial\theta} = 0 \quad \text{on} \quad \theta = \frac{\pi}{2} \tag{3}$$

$$\left[\frac{\partial\Phi}{\partial t} + \frac{1}{2}\left(\frac{\partial\Phi}{\partial r}\right)^2 + \frac{1}{2r^2}\left(\frac{\partial\Phi}{\partial\theta}\right)^2\right]_{r=R} = \frac{p_\infty - p_i}{\rho} \tag{4}$$

Discussion on this paper will be accepted at ASME Headquarters until June 10, 1961

where p_∞ and p_c are the constant pressures at infinity and in the cavity, respectively, and ρ is the liquid density.

$$\left[\frac{\partial \Phi}{\partial r} - \frac{1}{r^2}\frac{\partial \Phi}{\partial \theta}\cdot\frac{\partial R}{\partial \theta}\right]_{r=R} = \frac{\partial R}{\partial t} \tag{5}$$

where t is the time. A solution to Equation (1) which satisfies Equations (2) and (3) is

$$\Phi(r, \theta, t) = \frac{\phi_0(t)}{r} + \sum_{n=1}^{\infty} \phi_{2n}(t)\frac{1}{r^{2n+1}} P_{2n}(\cos\theta) \tag{6}$$

where $P_{2n}(\cos\theta)$ are Legendre polynomials, and ϕ_0 and ϕ_{2n} are time-dependent coefficients in the expansion. One is thus led to express

$$R(\theta, t) = R_0(t) + \sum_{n=1}^{\infty} R_{2n}(t)P_{2n}(\cos\theta) \tag{7}$$

where R_0 and R_{2n} are time-dependent coefficients in the expansion. The procedure for solution is then to substitute Equations (6) and (7) into Equations (4) and (5), thus obtaining the differential equations that must be satisfied by ϕ_0, ϕ_{2n}, R_0, and R_{2n}. These differential equations are then solved with the initial conditions.

$$R(\theta, 0) = R_0(0) + \sum_{n=1}^{\infty} R_{2n}(0)P_{2n}(\cos\theta) \tag{8}$$

$$\frac{dR}{dt}(\theta, 0) = \sum_{n=1}^{\infty} \frac{dR_{2n}}{dt}(0)P_{2n}(\cos\theta). \tag{9}$$

The quantities $R_0(0)$, $R_{2n}(0)$, and $\frac{dR_{2n}}{dt}(0)$ are specified. Time $t = 0$ is chosen such that $dR_0/dt = 0$.

In view of the nonlinearity of Equations (4) and (5), an attempt is made to obtain a perturbation solution for restricted values of the quantities ϕ_{2n} and R_{2n}.

First Perturbation Procedure. Assume that the sums on the right-hand sides of Equations (6) and (7) are small compared to ϕ_0/r and R_0, respectively, so that all interactions between terms in these sums may be neglected. Substituting Equations (6) and (7) into Equations (4) and (5), and using the orthogonality of Legendre polynomials, one finds

$$\phi_0 = \left[\frac{2}{3}\frac{p_\infty - p_c}{\rho} R_0(R_0^3(0) - R_0^3)\right]^{1/2} \tag{10}$$

$$t = \frac{R_0(0)}{\left[\frac{2}{3}\frac{p_\infty - p_c}{\rho}\right]^{1/2}} \int_{\frac{R_0}{R_0(0)}}^{1} \frac{d\xi}{\left[\frac{1}{\xi^3} - 1\right]^{1/2}} \tag{11}$$

The time at which R_0 becomes zero is given by

$$T = \frac{0.915R_0(0)}{\left[\frac{p_\infty - p_c}{\rho}\right]^{1/2}}. \tag{12}$$

The $P_0(\cos\theta)$ component of the bubble thus still satisfies the Rayleigh theory.

With the substitutions $\left[\frac{R_0(0)}{R_0}\right]^3 = x$ and $\frac{R_{2n}}{R_{2n}(0)} = y_{2n}$ the following equation is obtained for the R_{2n}:

$$(1 - x)x\frac{d^2y_{2n}}{dx^2} + \left(\frac{1}{3} - \frac{5}{6}x\right)\frac{dy_{2n}}{dx} - \frac{1}{6}(2n - 1)y_{2n} = 0. \tag{13}$$

Equation (13) is of hypergeometric form [4], with

$$c = \frac{1}{3}$$

$$a(n) = \frac{1}{12}(-1 + i(48n - 25)^{1/2}) \tag{14}$$

$$b(n) = \frac{1}{12}(-1 - i(48n - 25)^{1/2})$$

and the general solution can be written in the form [4]

$$y_{2n} = A_{2n}x^{-a}F\left(a, a + \frac{2}{3}; \frac{1}{2}; 1 - \frac{1}{x}\right) + B_{2n}x^{-a}(1 - x)^{1/2}F\left(-b + \frac{1}{3}; -b + 1; \frac{3}{2}; 1 - \frac{1}{x}\right) = A_{2n}y_{2n_1} + B_{2n}y_{2n_2} \tag{15}$$

where the hypergeometric function F is given by

$$F(\alpha, \beta; \gamma; z) = \sum_{m=0}^{\infty} \frac{(\alpha)_m(\beta)_m}{(\gamma)_m} z^m \tag{16}$$

and

$$(\alpha)_m = \Gamma(\alpha + m)/\Gamma(\alpha).$$

The constants A_{2n} and B_{2n} are readily determined from the initial conditions

$$A_{2n} = 1$$

$$B_{2n} = 0.892\frac{dy_{2n}}{d(t/T)}. \tag{17}$$

The solutions y_{2n_1} and y_{2n_2} are shown in Figs. 2 and 3, respec-

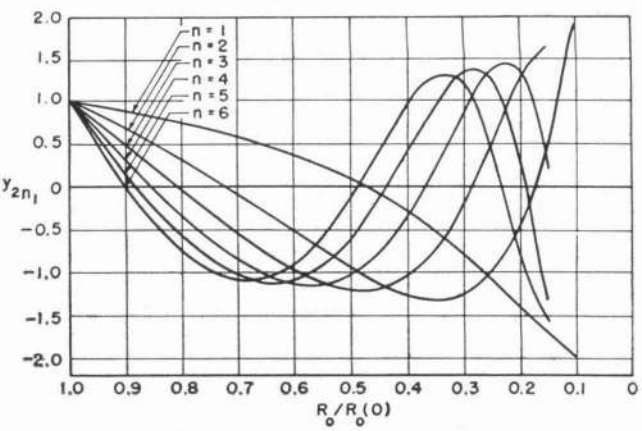

Fig. 2 The first solution to Equation (13), y_{2n_1}, as a function of $R_0/R_0(0)$

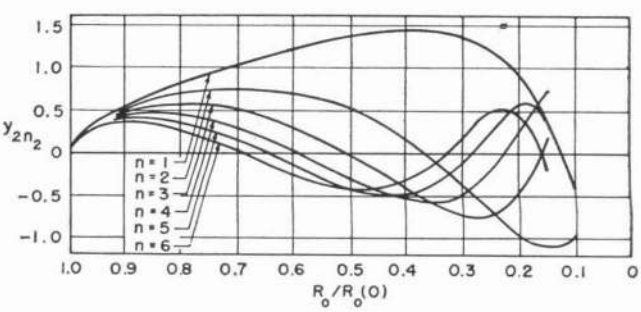

Fig. 3 The second solution to Equation (13), y_{2n_2}, as a function of $R_0/R_0(0)$

tively, as functions of $R_0/R_0(0)$. The solutions given here are the same as the one obtained by Plesset and Mitchell [1]. In the present case, odd Legendre polynomials have been eliminated because of the boundary. Both y_{2n_1} and y_{2n_2} exhibit an interesting characteristic, namely, that they oscillate with increasing amplitude and frequency as R_0 approaches zero. Physically this implies that a finite initial perturbation, $\sum_{n=1}^{\infty} R_{2n}P_{2n}$, of the hemispherical shape could grow so large that the cavity wall could strike the solid boundary before R_0 becomes zero. Because of the large perturbation quantities that are involved at this stage of collapse it is not possible to apply the simple theory that has been presented. As far as damage by cavitation is concerned, the suggestions offered by this theory are interesting enough to stimulate further investigation.

Second Perturbation Procedure. Consider a somewhat more physically realistic cavity for which $R_0 > R_2 > R_4 > R_6$, and R_{2n} is negligibly small for $n \geq 4$ in Equation (7). The most significant interactions between terms in the sums of Equations (6) and (7) will be retained in this analysis in an attempt to obtain a better description of the behavior of the cavity when perturbations of the hemispherical shape become fairly large.

One then finds that R_0 and ϕ_0 will satisfy Equations (10) and (11) within terms of order $\left[\frac{R_2(0)}{R_0(0)}\right]^2$.

$\frac{R_{2n}}{R_{2n}(0)} = y_{2n}'$ now satisfies

$$(1-x)x\frac{d^2y_{2n}'}{dx^2} + \left(\frac{1}{3} - \frac{5}{6}x\right)\frac{dy'_{2n}}{dx} - \frac{1}{6}(2n-1)y_{2n}' = F_{2n}(x) \quad \text{for } n = 1, 2, \text{ and } 3. \tag{18}$$

$$F_2 = 0 + O\left(\frac{R_2(0)}{R_0(0)}\right) \tag{19}$$

$$F_4 = -\frac{1}{315}\left[\frac{R_2^2(0)}{R_0(0)R_4(0)}\right](x^{-2/3})\left[(49x+32)y_2'^2 + 474(x-1)x\frac{dy_2'}{dx}y_2' - 639(x-1)x^2\left(\frac{dy_2'}{dx}\right)^2\right] + O\left(\frac{R_2(0)}{R_0(0)}\right) \tag{20}$$

$$F_6 = -\frac{1}{297}\left[\frac{R_0(0)R_4(0)}{R_2(0)R_6(0)}\right](x^{-2/3})\left[(129x+96)y_2'y_4' + 765(x-1)x\frac{dy_2'}{dx}y_4' + 639(x-1)xy_2'\frac{dy_4'}{dx} - 1485(x-1)x^2\frac{dy_2'}{dx}\frac{dy_4'}{dx}\right] + \frac{1}{3465}\left[\frac{R_2^3(0)}{R_0^2(0)R_6(0)}\right](x^{-1/3})\left[(3418x-4228)y_2'^3 - 17328(x-1)xy_2'^2\frac{dy_2'}{dx} + 19395(x-1)x^2y_2'\left(\frac{dy_2'}{dx}\right)^2\right] + O\left(\frac{R_2(0)}{R_0(0)}\right). \tag{21}$$

The only difference between Equations (13) and (18) is that (18) contains a forcing function F_{2n}. One may thus write

$$y_{2n}' = y_{2n} + y_{2np} \tag{22}$$

where y_{2np} is a particular integral of Equation (18). The particular integral can be found readily by variation of parameters [5]

$$y_{2np} = -u_{2n}\int_1^x \left[\frac{1}{u_{2n}^2(x-1)^{1/2}x^{1/3}}\int_1^x \frac{u_{2n}F_{2n}}{(x-1)^{1/2}x^{2/3}}dx\right]dx \tag{23}$$

where u_{2n} is a solution to the homogeneous Equation (13). The lower limits of the integrals have been chosen in such a way that y_{2np} and dy_{2np}/dt vanish initially, so that Equations (17) are still valid. The singularities of the integrals at $x = 1$ are integrable, and the singularities at the zeros of u_{2n} can be shown to be removable.

Because $F_2 = 0$, y_2' can be written in the form

$$y_2' = y_{2_1} + B_2y_{2_2} \tag{24}$$

The function F_4 can then be expressed

$$F_4 = \left[\frac{R_2^2(0)}{R_0(0)R_4(0)}\right][F_{4_1} + B_2F_{4_2} + B_2^2F_{4_3}] \tag{25}$$

so that

$$y_{4p} = \left[\frac{R_2(0)}{R_0(0)R_4(0)}\right][y_{4p_1} + B_2y_{4p_2} + B_2^2y_{4p_3}] \tag{26}$$

where

$$y_{4p_i} = -u_4\int_1^x \left[\frac{1}{u_4^2(x-1)^{1/2}x^{1/3}}\int_1^x \frac{u_4F_{4_i}}{(x-1)^{1/2}x^{2/3}}dx\right]x. \tag{27}$$

In Fig. 4 y_{4p_i}, with $i = 1$, 2, and 3, are shown as functions of $R_0/R_0(0)$. Fig. 5 is a magnification of the portions of these functions for which $R_0/R_0(0) > 0.4$.

In Fig. 6, theoretical cavity shapes at different values of $R_0/R_0(0)$ are demonstrated. The initial conditions for this cavity are the same as for the experimental cavity demonstrated in Fig. 18, and can be specified by $R_0(0) = 0.225$ in., $R_2(0) = 0.065$ in., $R_4(0) = -0.0127$ in., $B_2 = -0.83$, $B_4 = -5.45$, $T = 524\mu s$. The jet which enters the cavity and strikes the solid boundary is evident. The fact that the radius of curvature of the jet becomes zero at the time of impact is not physically realistic, and is probably the result of a breakdown of the perturbation procedure plus the fact that surface tension has been omitted from the theory.

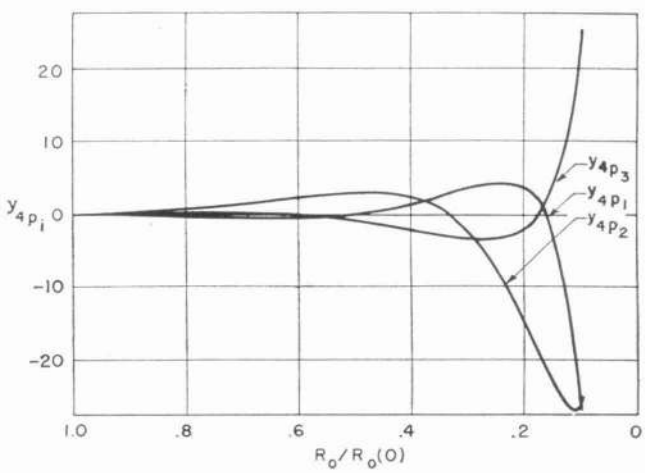

Fig. 4 The three components of the particular integral of Equation (18) with $n = 2$

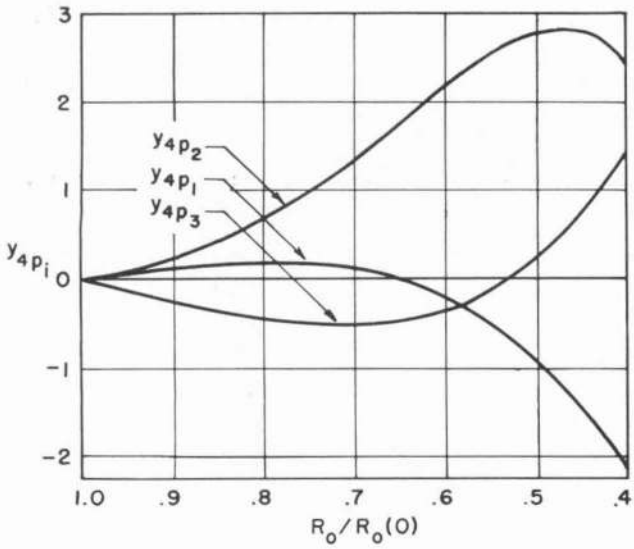

Fig. 5 The three components of the particular integral of Equation (18) with $n = 2$ for $R_0/R_0(0)$ 0.4

The Validity of the Assumptions

1 An estimate of the error introduced by neglecting compressibility can be obtained from the work of Gilmore [6]. For a cavity collapsing in water under a constant pressure difference of 1 atm, the error in cavity radius reaches about 10 per cent when $R_0/R_0(0) = 0.1$.

2 For a vaporous cavity the assumption of constant cavity pressure will become poor when the cavity wall velocity becomes comparable to the velocity of the vapor molecules at the temperature inside the cavity. Assuming isothermal collapse, which is probably pessimistic, the assumption will become poor for a cavity in water when the wall velocity reaches 2000 ft/sec. With a pressure difference of 1 atm, this corresponds to $R_0/R_0(0) = 0.05$.

3 A rough estimate of the effect of viscosity can be obtained by using the two-dimensional boundary-layer theory for a suddenly accelerated plane wall. The boundary-layer thickness δ is given by [7] $\delta \approx 4\sqrt{\nu t}$ where ν is the viscosity and t is the time after the motion began. Replacing t with T from Equation (12) one finds that for cavities with $R_0(0) > 0.1$ in. in water, the boundary-layer thickness will reach at most 20 per cent of R_0 when $R_0/R_0(0)$ becomes 0.15, provided the pressure difference is 1 atm. The effect becomes much smaller as $R_0(0)$ is increased.

4 A comparison of surface tension forces with inertia forces shows that, for bubbles collapsing in water, under 1 atm pressure difference, radii of curvature of the order of 10^{-9} ft have to occur at $R_0/R_0(0) = 0.05$ before these forces become comparable.

5 A rough calculation based on the work of Cole [8] shows that the effect of the solid boundary greatly supersedes the effect of gravity for cavities of the type considered here.

Experimental Results

Because the convergence of the perturbation theory which was presented could not be proved, and because perturbation quantities become very large during the final stages of collapse, it seemed necessary to perform some experiments to cast more light on the subject.

A series of motion pictures of cavities generated by spark methods were taken with the Ellis Kerr cell camera [9]. The magnitude of the perturbation of the hemispherical shape was varied by simply changing the distance of the spark gap from the solid boundary. Since indented portions of the cavity wall could not be photographed, an indirect means of observing the jet entering the cavity had to be found. Use of a photoelastic solid boundary proved to be the most successful method.

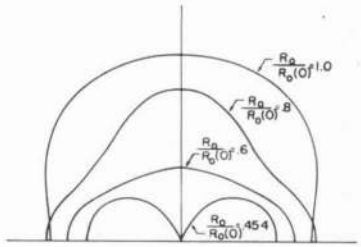

Fig. 6 Theoretical cavity shapes for different values of $R_0/R_0(0)$

In Fig. 7 a typical motion-picture record of a cavity collapsing on a CR-39 photoelastic boundary is presented. Frames below one another in vertical columns are consecutive, and columns follow one another from left to right. R_0, R_2, R_4, and R_6 as functions of time were found from a Legendre analysis of the motion pictures. R_0 reached its maximum of 0.244 in. in frame 9 of the first column. At this time, $R_2(0)$ and $R_4(0)$ were 0.113 and -0.0334 in., respectively. B_2 and B_4 had the values -0.57 and -2.4. The time for complete collapse T was approximately 570 μs. The small disturbance which originates near the center of the cavity base in frame 12 of column 5 is believed to be the result of the impinging jet.

The large disturbance in frame 9 of column 6 probably corresponds to the compression of gases in the cavity, because afterward the cavity volume increases again.

In Figs. 8, 9, and 10 experimental points of $R_0/R_0(0)$ as a function of time, and $R_2/R_2(0)$ and $R_4/R_4(0)$ as functions of $R_0/R_0(0)$ are compared with the theory. Dotted vertical lines in these figures indicate when the cavity became indented. Points to the right of the dotted lines depend on an estimate of the shape of the indented portion which was greatly aided by a knowledge of when the jet struck the solid boundary. The dotted curve in Fig. 10 shows the results of the first perturbation procedure, while the solid curve was calculated by means of the second perturbation method. Agreement between theory and experiment for this particular cavity was better than average. Considering the scatter of the experimental data, agreement was good in the range of cavities which were considered.

In Figs. 11 and 12 an attempt was made to obtain a simultaneous comparison of $R_2/R_2(0)$ for ten different cavities with the theory. Such a comparison is necessarily based on an apportioning of the difference between theory and experiment to the y_{2_1} and y_{2_2} parts of $R_2/R_2(0)$. The method of apportioning that was used is as follows:

Suppose that at $R_0/R_0(0) = \omega$, an experimental value of $R_2/R_2(0)$ was found to be y_{2e}. The difference ϵ between theory and experiment at this point is then

$$\epsilon = y_2(\omega) - y_{2e}(\omega) = y_{2_1}(\omega) + B_2 y_{2_2}(\omega) - y_{2e}(\omega).$$

One may then write

$$y_{2e}(\omega) = \left[y_{2_1}(\omega) - \epsilon \frac{|y_{2_1}(\omega)|}{|y_{2_1}(\omega)| + |B_2 y_{2_2}(\omega)|} \right] + B_2 \left[y_{2_2}(\omega) - \epsilon \frac{|B_2|}{B_2} \frac{|y_{2_2}(\omega)|}{|y_{2_1}(\omega)| + |B_2 y_{2_2}(\omega)|} \right]$$

$$= y_{2e_1}(\omega) + B_2 y_{2e_2}(\omega).$$

The "experimental" points of y_{2e_1} and y_{2e_2} are then compared with the theory.

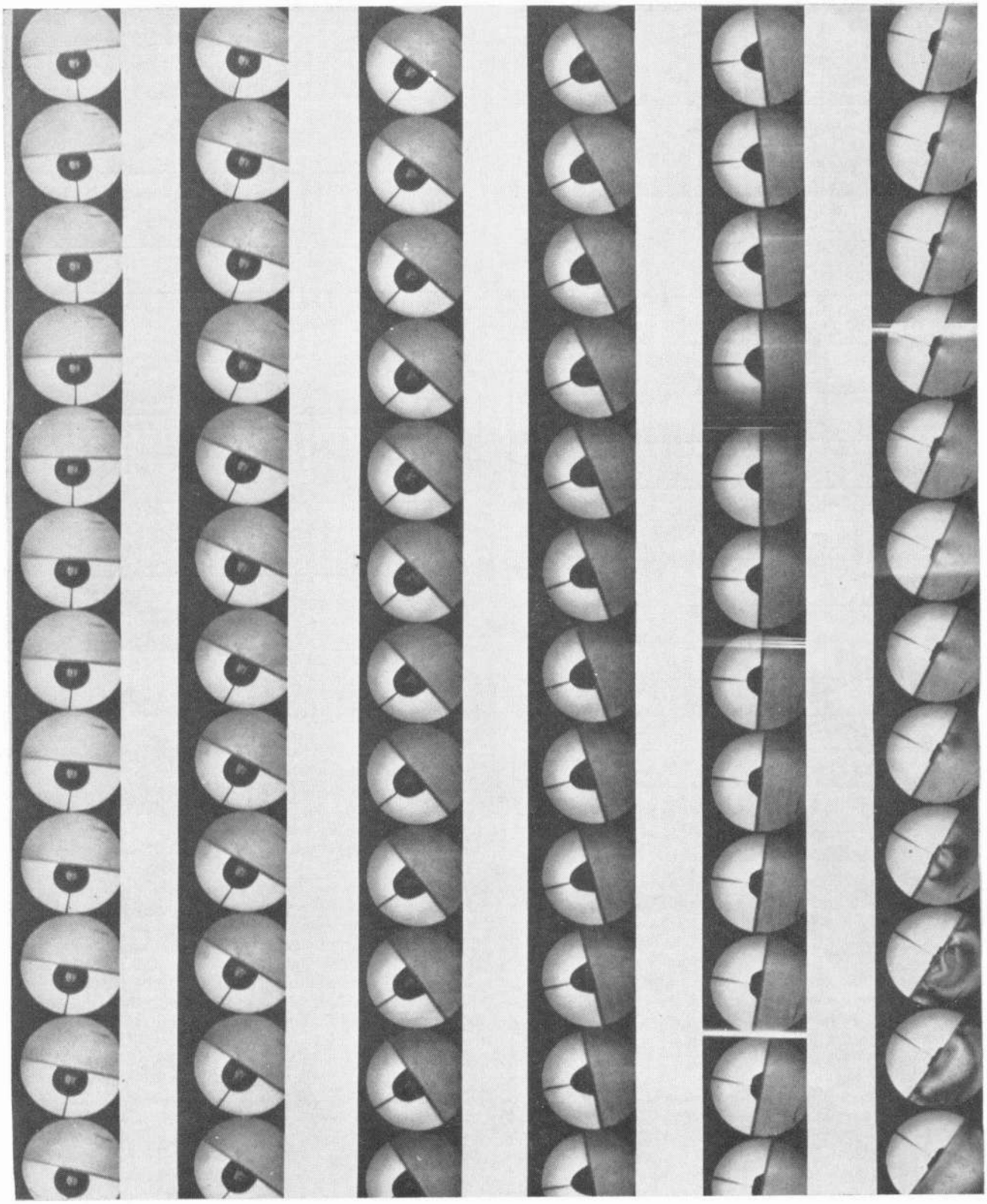

Fig. 7 A cavity collapsing on the CR-39 photoelastic boundary. Time between frames is 10 microsec.

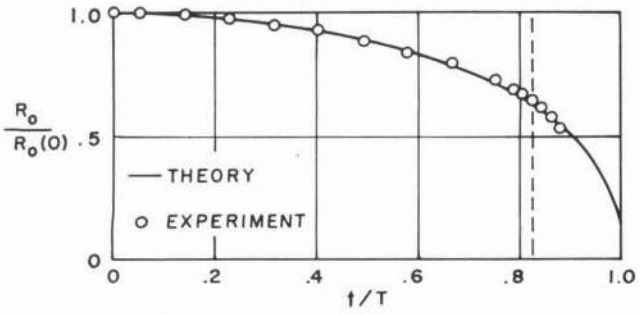

Fig. 8 $R_0/R_0(0)$ as a function of t/T for the cavity in Fig. 7

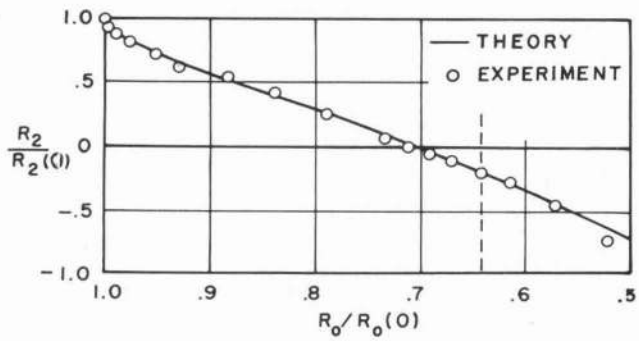

Fig. 9 $R_2/R_2(0)$ as a function of $R_0/R_0(0)$ for the cavity in Fig. 7

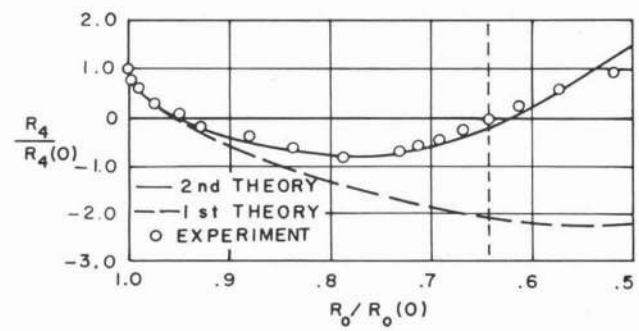

Fig. 10 $R_4/R_4(0)$ as a function of $R_0/R_0(0)$ for the cavity in Fig. 7

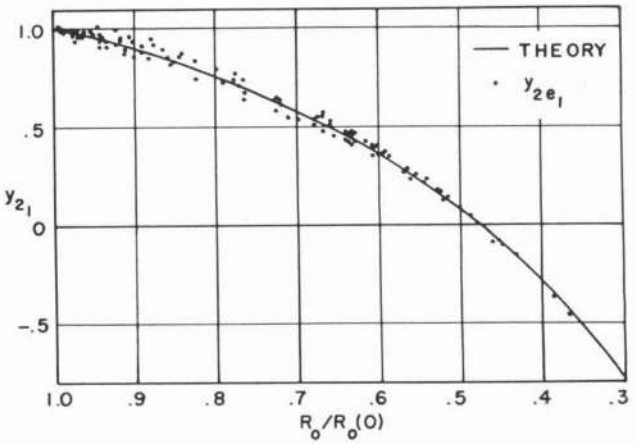

Fig. 11 A comparison of experimental points for y_{2e_1} with the theoretical y_{2_1} curve

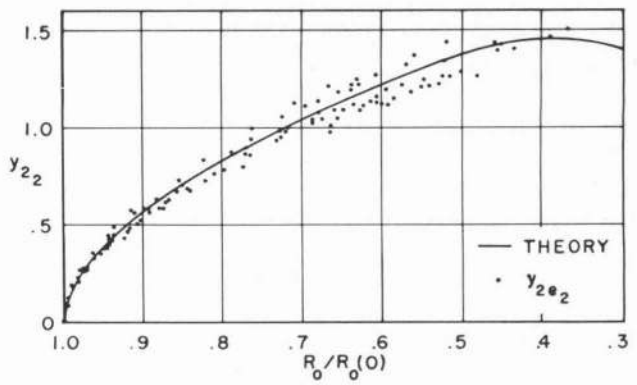

Fig. 12 A comparison of experimental points for y_{2e_2} with the theoretical y_{2_2} curve

Despite the evident weakness of the method of apportioning, Figs. 11 and 12 give a good indication of the scatter involved in the experimental results. The experimental points seem to be well grouped around the theoretical curves.

A similar representation of experimental results for $R_4/R_4(0)$ was not attempted, because y_4 is a linear combination of five different functions of $R_0/R_0(0)$.

Experimental data for $R_6/R_6(0)$ were very erratic because the magnitude of y_6 was of the same order as errors in the measurements. These results are not presented.

Although the photoelastic fringes (isochromatics) were of great value in determining the time at which a jet struck the solid boundary, it was not possible to derive quantitative information regarding the pressures which occurred from the fringe patterns because the area over which the pressure acted and the pressure distribution were unknown. Some quantitative information regarding the magnitude of the compression pulse could be obtained with the use of a quartz crystal pressure pickup.

The pickup is shown schematically in Fig. 13. The crystal Q is glued into the end of an aluminum bar which is made up of tubes C_1, C_2, C_3, and the rod C_4. All these elements are electrically nsulated from one another, and thus form connections to four different areas on the back of the crystal. The insulation of C_1, C_2, C_3, and C_4 was achieved by anodizing them before they were glued together. The aluminum plate P forms the connection to the front of the crystal. Troubles from reflections were minimized by lead bar L which was glued to the other end of the unit. Electrical connections to C_2, C_3, and C_4 are obtained with wires through size 80 holes drilled down the center of 0-80 nylon screws S_2, S_3, and S_4. An 0-80 brass screw S_1 forms the connection to C_1.

In Fig. 14 the output obtained from C_2 (upper trace) and C_4 (lower trace) with C_1 and C_3 grounded is shown when a $^1/_{16}$ in. ball bearing is dropped through 2 in. on the center of the crystal. The vertical scale is 0.005 volts per div while the horizontal scale is 10μs per div. A 25 megacycle X-cut quartz crystal was used in obtaining these curves. The pickup was originally constructed for purposes of measuring the impact of the jet on the boundary. For this purpose it was a complete failure, because even the $^1/_{16}$ in. diam center area was much larger than the jet, and also because of poor high-frequency response. It did, however, provide a means of measuring the pressure of the gases in the cavity, because the minimum base diameter of the cavities were larger than $^1/_{16}$ in., and the frequencies involved were not as high.

Experimental measurements of pressures resulting from a compression of gases in the cavity at different spark gap distances from the solid boundary are shown in Fig. 15. The spark energy was kept constant during these observations and spherical cavities which were produced had a maximum radius of approximately 0.16 in. Fig. 16 shows a picture of the cavity corresponding to

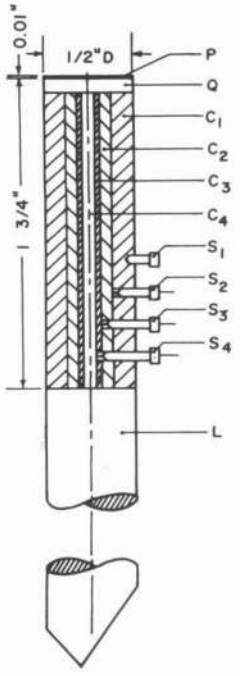

Fig. 13 The quartz crystal pickup

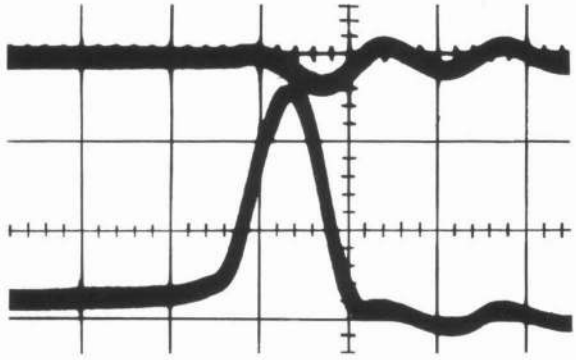

Fig. 14 The response of the quartz crystal unit to a $^1/_{16}$ in. ball bearing dropped on the center of the crystal

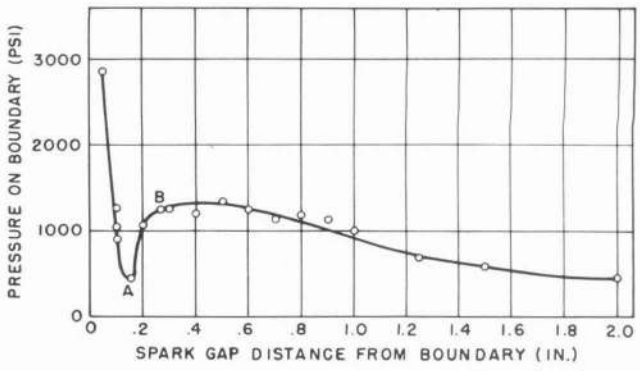

Fig. 15 Pressures on the solid boundary arising from a compression of gases in the cavity

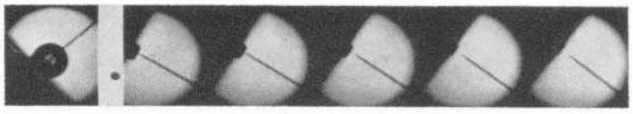

Fig. 16 The cavity corresponding to point A in Fig. 15

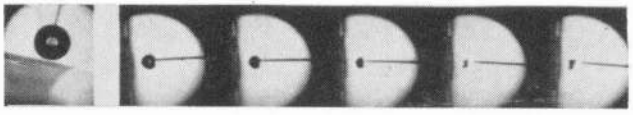

Fig. 17 The cavity corresponding to point B in Fig. 15

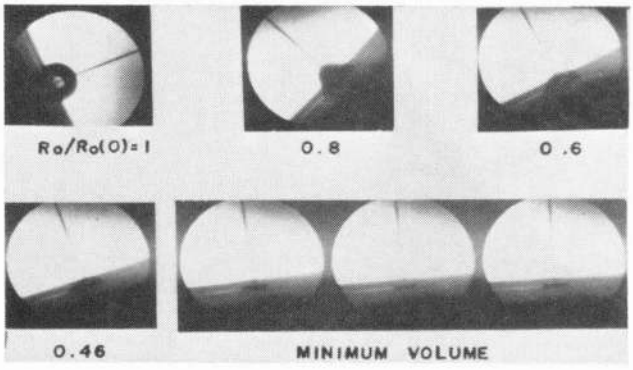

Fig. 18 A cavity used in the damage studies

point A of Fig. 15 at maximum R_0, and a few frames at the time of the compression pulse. Fig. 17 shows the same frames for the cavity corresponding to point B in Fig. 15.

It is seen that pressures on the boundary resulting from a compression of gases inside the cavity for cavities in contact with the boundary decrease rapidly as the perturbation of the hemispherical shape is increased. This is probably because the collapse process becomes less spherically symmetric. The pressure starts rising again when the distance of the spark gap from the boundary becomes large enough so that the cavities collapse away from the boundary, and the collapse becomes more spherically symmetric. A maximum is reached when the gain in pressure due to more spherically symmetric collapse is canceled by the inverse square dropoff with increasing distance from the boundary and afterward pressures on the boundary diminish gradually. It is of interest to note that shock-wave pressures on the boundary can be higher than pressures resulting from a compression of gases of cavities which collapse on the boundary. These shock-wave pressures are, however, quite low for the spark bubbles which were considered here, and although such pressures could increase greatly if cavities contained less permanent gas, it seems unlikely that shock waves will play an important role in cavitation damage.

The only information regarding the impact of the jet on the solid boundary was obtained from a study of the damage by cavities of this nature on aluminum samples. Fig. 18 shows a typical cavity used in the damage studies at $R_0/R_0(0)$ values of approximately 1.0, 0.8, 0.6, and 0.46, and close to minimum volume. The pit produced by this cavity in an annealed and chemically polished high purity aluminum sample is shown in Fig. 19. The scale in Fig. 18 is 0.004 in. per div, and the minimum base diameter of the cavity in Fig. 19 is 0.179 in. The pit diameter is thus only $^1/_{15}$ of the minimum cavity base diameter, so that the possibility that the pit could have been caused by a compression of the gases in the cavity can be ruled out, and the impact of the jet must have been responsible.

Damage studies of this nature yielded some information that cannot easily be explained in terms of the predicted mechanism. Cavities with somewhat larger initial perturbations of the hemi-

spherical shape than the one shown in Fig. 18 failed to cause visible damage of the soft aluminum samples. For these cavities the estimated impact velocities of the jet were higher than the 300 ft/sec which was estimated for the cavity in Fig. 18. Another parameter thus appears to be playing a role as far as the damage is concerned. It was speculated that this parameter could be the radius of curvature of the tip of the jet.

A reduction of the initial perturbations of the hemispherical shape to values smaller than those of Fig. 18 drastically increased the damage potential of the cavities. A single cavity with $R_0(0) = 0.232$ in., $R_2(0) = 0.012$ in., $R_4(0) = 0.0114$ in., $B_2 = -3.25$, $B_4 = 2.00$, and $T = 524\mu s$ could produce a pit in an aluminum, alloy with a yield strength of 50,000 psi. No experimental explanation for this increase in the impact pressure could be found because the detailed behavior of the indented portions of the cavity wall could not be observed. The theory suggests a possible explanation which will be discussed briefly. The theoretical curves of $R_2/R_2(0)$ and $R_4/R_4(0)$ for this cavity are demonstrated in Figs. 20 and 21. The distance D of the tip of the jet from the solid boundary is shown in Fig. 22 as a function of $R_0/R_0(0)$. The dotted line in this figure corresponds to the cavity of Fig. 18.

It is thus seen that in the present situation, the jet which enters the cavity performs one complete oscillation before it strikes the boundary, while the jet entering the cavity in Fig. 18 continues its motion toward the boundary until the impact occurs. This oscillatory behavior could be the reason for the increased damage potential that was observed, because the impact velocity is greatly increased. The theoretical impact velocity in this case is 3350 ft/sec as compared to a mere 300 ft/sec for the cavity in Fig. 18.

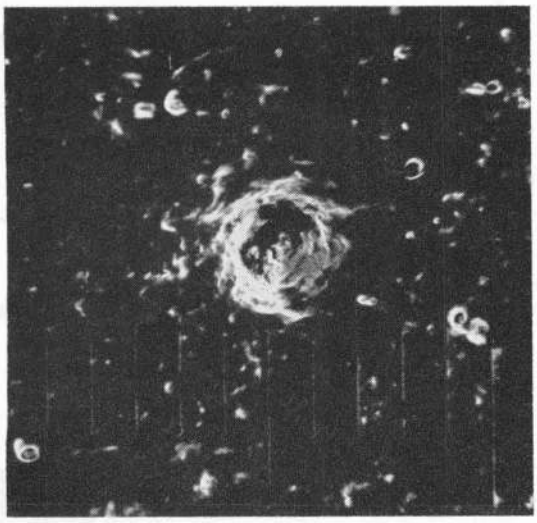

Fig. 19 The pit produced in high purity aluminum by the cavity in Fig. 18

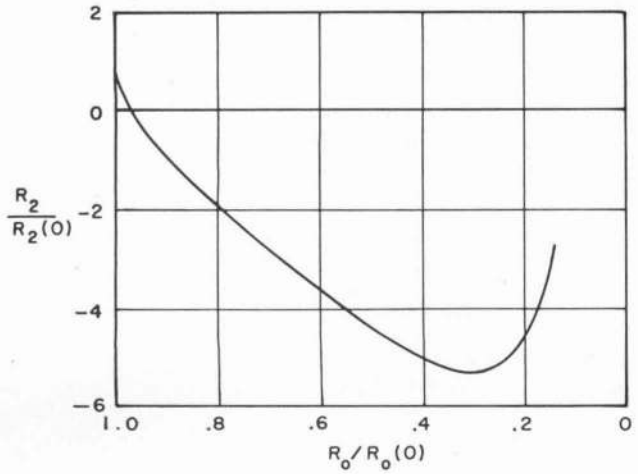

Fig. 20 $R_2/R_2(0)$ as a function of $R_0/R_0(0)$ for the second cavity discussed under the damage studies

Conclusions

1 Experimental results on the shape of cavities collapsing in contact with a boundary confirmed the theory derived by means of the second perturbation procedure.

2 Jets which enter cavities and damage the solid boundary through direct impact were observed experimentally. The occurrence of these jets is in agreement with suggestions of the theory.

3 The theory provided a partial explanation of the increase in damage potential of cavities when initial perturbations of the hemispherical shape were reduced. In addition to the impact velocity of the jet, another parameter, possibly the radius of the tip of the jet, seemed to influence the damage.

4 Shock wave pressures due to cavities of 0.16 in. radius collapsing away from the solid boundary under 1 atm pressure difference were measured. These pressures had a maximum of about 1300 psi, and even though spark bubbles may contain more permanent gas than actual cavitation bubbles, it appears unlikely that cavities collapsing away from a boundary play an important role in cavitation damage.

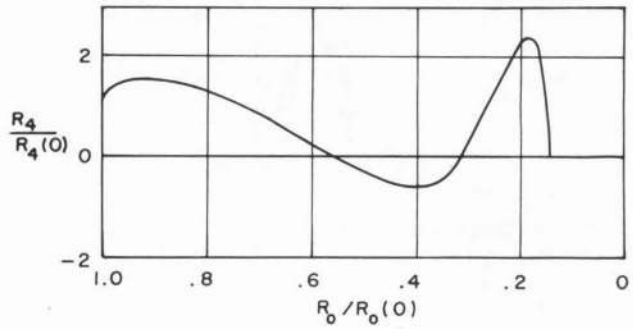

Fig. 21 $R_4/R_4(0)$ as a function of $R_0/R_0(0)$ for the second cavity discussed under the damage studies

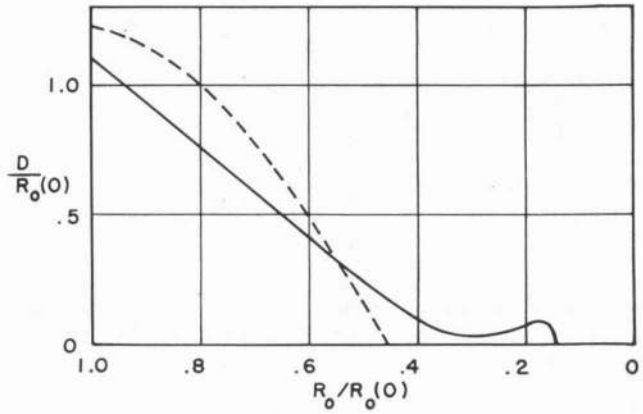

Fig. 22 The reduced distance $D/R_0(0)$ of the tip of the jet from the solid boundary for the two cavities discussed under the damage studies

Acknowledgments

The authors wish to express their sincere appreciation for the competent assistance of Prof. P. A. Lagerstrom with the theoretical work.

Financial support from the following sources made this study possible:

1 Research Bursary from the South African Council for Scientific and Industrial Research (1956–1959).

2 Queen Victoria Stipendium from the University of Stellenbosch, South Africa (1957–1959).

3 Francis J. Cole Fellowship from the California Institute of Technology.

The experimental work was carried on with support from:

1 National Science Foundation Grant G-2586.

2 U. S. Navy Bureau of Ordnance contract NOrd 16200.

3 Office of Naval Research equipment loan NOnr 218100.

4 U. S. Naval Ordnance Test Station Contract N123(60530)-21703A.

5 U. S. Naval Ordnance Test Station Contract N123(60530)-24917A

References

1 M. S. Plesset and T. P. Mitchell, "On the Stability of the Spherical Shape of a Vapor Cavity in a Liquid," *Quarterly of Applied Mathematics*, vol. 13, 1956, pp. 419–430.

2 P. Eisenberg, "On the Mechanism and Prevention of Cavitation," David Taylor Model Basin, Report 712 (1950), pp. 51–52.

3 M. Kornfeld and L. Suvorov, "On the Destructive Action of Cavitation," *Journal of Applied Physics*, vol. 15, no. 6, 1944, pp. 495–496.

4 Erdelyi, et al., "Higher Transcendental Function," vol. 1, McGraw-Hill Book Company, Inc., New York, N. Y., 1958, pp. 56, 105–106.

5 H. Wayland, "Differential Equations in Science and Engineering," D. Van Nostrand Company, New York, N. Y., 1957, p. 120.

6 F. R. Gilmore, "The Growth or Collapse of a Spherical Bubble in a Viscous Compressible Liquid," California Institute of Technology, Hydrodynamics Laboratory Report 26-4, 1952.

7 H. Schlichting, "Boundary Layer Theory," McGraw-Hill Book Company, Inc., New York, N. Y., 1955, pp. 64–65.

8 R. H. Cole, "Underwater Explosions," Princeton University Press, 1948, pp. 338–341.

9 A. T. Ellis, "Observations on Cavitation Bubble Collapse," California Institute of Technology, Hydrodynamics Laboratory Report 21-12, 1952

Printed in U. S. A.